Computationally Identified Novel Chemical Compounds that Antagonize FGF-23

Z. S. Xiao[1], D. Riccardi[2,5], H. A. Velazquez[3,6], A. L. Chin[5], C. R. Yates[4], J. D. Carrick[5], J. C. Smith[3,6], J. Baudry[3,6], L. D. Quarles[1,*]

One Sentence Summary: Identification of novel FGF-23 antagonists

Affiliations:

[1]Department of Medicine, College of Medicine, University of Tennessee Health Science Center, Memphis, TN, 38165, USA

[2]Department of Chemistry, Earlham College, 801 National Road West, Richmond, Indiana 47374, USA

[3]UT/ORNL Center for Molecular Biophysics, Oak Ridge National Laboratory, 1 Bethel Valley Road, Oak Ridge, Tennessee 37830, USA

[4]Department of Pharmaceutical Sciences**,** College of Pharmacy, University of Tennessee Health Science Center, Memphis, TN, 38163, USA

[5]Department of Chemistry, Tennessee Technological University, 55 University Drive, Cookeville, Tennessee 38501, USA

[6]Department of Biochemistry and Cellular and Molecular Biology, University of Tennessee, Knoxville TN 37996, U.S.A.

*Corresponding author:

Leigh Darryl Quarles, M.D.

Coleman College of Medicine Building, Suite B216

University of Tennessee Health Science Center

956 Court Avenue

Memphis TN 38163

email: dquarles@uthsc.edu

Phone: (901)-448-1459

Fax: (901)-448-1188

ABSTRACT

Fibroblast growth factor 23 (FGF-23) interacts with a binary receptor complex comprised of α-Klotho (α-KL) and fibroblast growth factor receptors (FGFRs) to regulate phosphate and vitamin D metabolism by the kidney. There is an unmet need to treat disorders of FGF-23 excess by modulating FGF-23 activation of the FGFR/α-KL complex. Here, we used a computationally driven, structure-based, ensemble docking, and virtual high-throughput screening approach to rationally identify four novel compounds that inhibit FGF-23 activation of the FGFR/α-KL L complex. Additional modeling and functional analysis found that Zinc13407541 binds to FGF-23 to disrupt its interaction with the FGFR1/α-KL complex, and selectivity inhibits α-KL dependent FGF-23 signaling in a heterologous cell expression system. Zinc13407541 also inhibited FGF-23 signaling in isolated renal tubules *ex vivo*, and partially reversed the hypophosphatemic effects of excess FGF-23 in animal models. These chemical probes provide a platform to develop lead compounds to treat disorders caused by FGF-23 excess.

INTRODUCTION

Fibroblast growth factor 23 (FGF-23) is a member of the subfamily of hormonal FGF ligands that includes FGF-19 and FGF-21 (*1*). FGF-23 is secreted by osteoblasts and osteocytes in bone and circulating FGF-23 participates in several endocrine signaling networks by targeting fibroblastic growth factor receptor (FGFR) and the type I membrane β-glycosidase α-Klotho (α-KL) that constitute the FGF-23 receptor (*2-7*). Specifically, the N-terminal FGF-homology domain of FGF-23 interacts with binding domains in FGFRs and its unique 71-residue C-terminus binds to α-KL, an obligate co-receptor for FGF-23 (*7-10*). α-KL forms a binary complex with FGFR1c, 3c, or 4, but not FGFR2, to form functional FGF-23 receptor complexes in a limited number to tissues (*11*). This eliminates the requirement for heparin binding for receptor activation that characterizes paracrine FGFs. α-KL is mainly expressed in the kidney, parathyroid gland, and choroid plexus thereby imparting selective FGF-23 activation of these tissues (*12-16*).

The major physiological functions of FGF-23 are to inhibit phosphate reabsorption and suppress 1,25$(OH)_2$D production in the proximal tubule of the kidney (*2, 10, 17-20*). However, FGF-23 also targets the distal renal tubule to stimulate renal sodium and calcium retention (*21-23*). Primary elevations of circulating FGF-23 concentration cause hereditarily acquired hypophosphatemic disorders, including X-linked hypophosphatemia (XLH), autosomal dominant (ADH) and autosomal recessive (ARH) hypophosphatemia, and tumor induced osteomalacia (TIO) (*18, 24-27*). FGF-23 is also purported to suppress parathyroid hormone secretion from the parathyroid gland that expresses FGFR/α-KL complexes (*28*). In contrast, reductions in circulating FGF-23 concentration causes familial tumoral calcinosis and leads to early postnatal mortality due to hyperphosphatemia and excessive1,25$(OH)_2$D production (*4, 29-34*).

Secondary elevations of FGF-23 contribute to the pathogenesis of mineral metabolism and cardiovascular disorders in chronic kidney disease (CKD) (*35*). Increased circulating concentrations of FGF-23 play an initial adaptive role in maintaining phosphate balance in chronic kidney

disease (*36, 37*), but become maladaptive with more advanced renal failure and are a strong independent risk factor for both renal failure progression and cardiovascular mortality (*38-40*).

Currently available treatments for hereditary hypophosphatemic disorders typically include calcitriol and phosphate supplements that are marginally effective and associated with side effects (*41*), including further stimulation of FGF-23 production (*42, 43*). Similarly, efforts to suppress secondary elevations of FGF-23 in CKD with phosphate binders and calcimimetics have been used with limited success (*44*). Inhibition of FGF-23 activation of FGFR/α-KL receptor complexes is likely to be a clinically important treatment for hereditary and acquired hypophosphatemic disorders, and may prevent cardiovascular complications associated with CKD. Indeed, a recombinant human IgG_1 monoclonal antibody that binds to FGF-23 and blocks the biologic activity of FGF-23 has been shown to be effective in treating hypophosphatemia in both animal models and humans with X-linked hypophosphatemic rickets(*45*). The long duration of action and requirement for systemic administration of FGF-23 blocking antibodies potentially limits their use to treat disorders of FGF-23 excess. There is an important unmet medical need to develop small molecule antagonists of FGF-23/FGFR/α-KL signaling to treat disorders of FGF-23 excess (*46-48*).

FGFR tyrosine kinase inhibitors, which have been shown to block both the production and end-organ effects of FGF-23, lack selectivity for FGF-23/FGFR/α-KL signaling, and their generalized ability to inhibit FGFRs in multiple tissues would have undesirable effects (*49, 50*). A small molecule, SSR128129E (SSR), which binds to the extracellular part of FGFR, was reported to act as a FGFR antagonist (*51*), but at present, there are no small molecules that specifically modulate FGF-23 activation of FGFR/α-KL complexes. The discovery of such molecules would not only provide research tools to elucidate FGF-23 biological actions, but also would advance the discovery of new treatments based on this novel bone/kidney endocrine network.

In the current study, a computationally-driven drug discovery approach employing homology modeling, molecular dynamics (MD) simulations and docking was used to rationally identify

small-molecules that modulate FGF-23 activation in the presence of FGFR1 and α-KL. MD simulations generated an ensemble of structures of the N-terminal domain of FGF-23, which were used to perform *in-silico* virtual screening to identify candidate molecules that dose-dependently and selectively inhibited FGF-23 activation of the FGFR1/α-KL complex in both *in vitro* cell culture and *in vivo* animal models.

RESULTS

Identification of trial compounds

First, we performed structural modeling of FGF-23 and generated homology models for molecular dynamic (MD) simulations to identify compounds that bind to FGF-23. The bioactive region of FGF-23 is from residues A28 through I251 and contains N-terminal and C-terminal (FGF-23CT) domains (*52*). The crystal structure of FGF-23 from S29 through N170, corresponding to the N-terminal domain, has been solved (*53*). FGF-23CT spans S180 through I251, demarcated by an RXXR179 furin like cleavage motif involved in FGF-23 metabolism (*54*). Residues S180 to T200 in the C-terminus are critical for binding α-KL (*52, 53*), and a 21-residue peptide derived from the FGF-23CT inhibits the activity of FGF-23 (*52*). Analysis of FGF-23 with the DISOPRED webserver (*55, 56*) indicates that the C-terminal domain is disordered **(Fig. 1A)**, consistent with the failure to crystallize the C-terminal domain (*53*). Hence, structural modeling was confined to the N-terminal domain. Homology models were generated with different initial configurations of the backbone and short, constrained MD simulations were performed to refine the structural models. The refined homology models used for the *in-silico* virtual screen show some diversity in backbone structure and side chain conformational variability, indicating that protein flexibility is accounted for to a limited extent in this analysis (**Fig. 1B**). We used the refined models for *in-silico* virtual screening

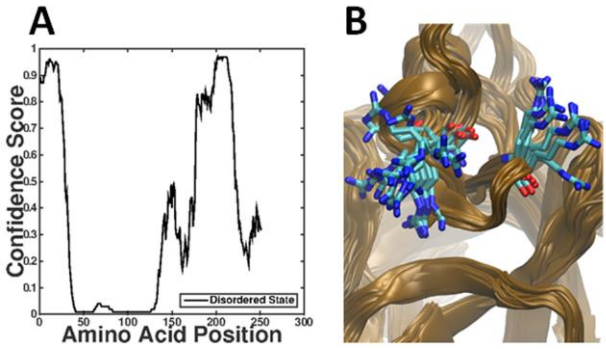

Fig. 1. FGF-23 homology modeling and *in-silico* virtual screen. (**A**) Intrinsic disorder profile of FGF-23 as predicted by DISOPRED3. (**B**) Side chain variability of Arg140 captured in the refined homology models.

to identify compounds predicted to bind to the N-terminal domain, screening both the NCI Diversity Set 2 and ZINC databases. We screened the ZINC database with a Tanimoto similarity cutoff of 0.8 (*57, 58*). The Tanimoto cutoff was used to search a subset of chemical diversity space that is uniquely different from the NCI Diversity Set 2. This resulted in a custom database of 84,589 compounds for computational screening. We selected chemical compounds for experimental validation based on these docking results, and tested the best scoring compounds in the experimental signaling assay below.

FGF-23 activation of FGFR1/α-KL signaling assay

In order to identify compounds generated from the *in-silico* virtual screening that antagonize FGF-23 actions, we established an *in vitro* screening assay to test the inhibitory effects of these chemical probes in the HEK-293 cells that express endogenous *FGFR1* and were engineered to overexpress *α-KL* transcripts (*11, 59, 60*) and Elk1-GAL reporter constructs

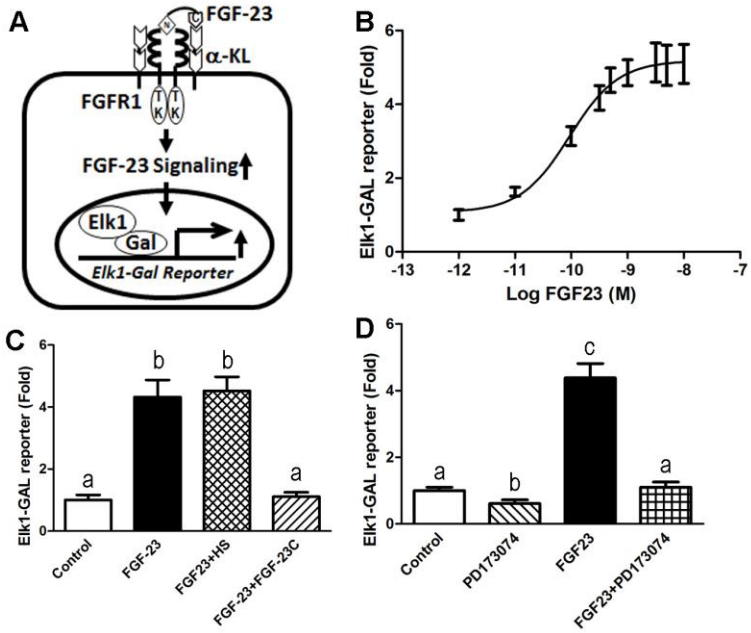

Fig. 2. Activation of FGF-23 signaling in HEK-293 cells that were transfected with human membrane *α-KL*. (**A)** Schematic of assay system. (**B)** Dose-response curve of FGF-23 mediated Elk1-GAL Luciferase activities; (**C)** Inhibitory effects of FGF-23 C-termineral (FGF-23C) on FGF-23 signaling; (**D)** The inhibitory effects of FGFR1 tyrosine kinase (TK) inhibitor (PD173074) on FGF-23 induced Gal-Elk1 reporter activities. Data are expressed as mean ± S.D. from three independent experiments. Values sharing the same superscript in different groups are not significantly different at $P<0.05$.

(**Fig 2A**). We validated this screening assay by demonstrating that exogenously added recombinant FGF-23 (rFGF23) stimulated Elk1-GAL luciferase reporter activity in a dose-dependent manner (**Fig. 2B**). The EC_{50} of rFGF-23 was ~0.1 nM (10^{-10} M). The maximal effect of rFGF-23 stimulating Elk1-Gal reporter activity was achieved at 1 nM (10^{-9} M). To validate this assay, we showed that heparin sulfate (HS) had no additive effect on rFGF-23 activation, while an FGF-23C blocking peptide (100 nM) completely abolished FGF-23 signaling (**Fig. 2C**). In addition, we found that FGFR1 tyrosine kinase (TK) inhibitor (PD173074, 10 μM) also abolished FGF-23-induced Gal-Elk1 reporter activities (**Fig. 2D).**

Identification of chemical probes that antagonize FGF-23-mediated activation of FGFR1/α-KL complex signaling in vitro

Using the above *in vitro* screening assay, we experimentally tested 16 high-scoring chemical probes identified from the *in-silico* virtual screen at an initial concentration of 10 μM in the absence and presence of rFGF-23 (**Fig 3**). Thirteen of the 16 compounds exhibited measurable effects inhibiting rFGF-23 stimulated Ekl1-Gal reporter activity (**Fig. 3**). Compounds NCI_61610, NCI_80313, and NCI_374204 at 10 μM concentration had no effect on FGF-23-induced signal transduction. Compounds Zinc04769985, NCI_37553, NCI_102656, NCI_401490, Zinc00055523, NCI_293778, NCI_308835, NCI_84100, and NCI_93354 at 10 μM concentration exhibited partial (less than 50%) inhibition of FGF-23-induced Gal-Elk1 reporter activity, and compound Zinc01626100 achieved an intermediate (~ 60%) inhibitory effect on FGF-23-induced signal transduction. However, compounds Zinc13407541, NCI_116702, and NCI_97920 completely suppressed FGF-23-induced Gal-Elk1 reporter activity at a 10-μM concentration (**Fig 3**). Only compounds NCI_97920 and NCI_116702 were found to inhibit basal FGFR1-α-KL activity in the absence of FGF-23 (**Fig. 3**).

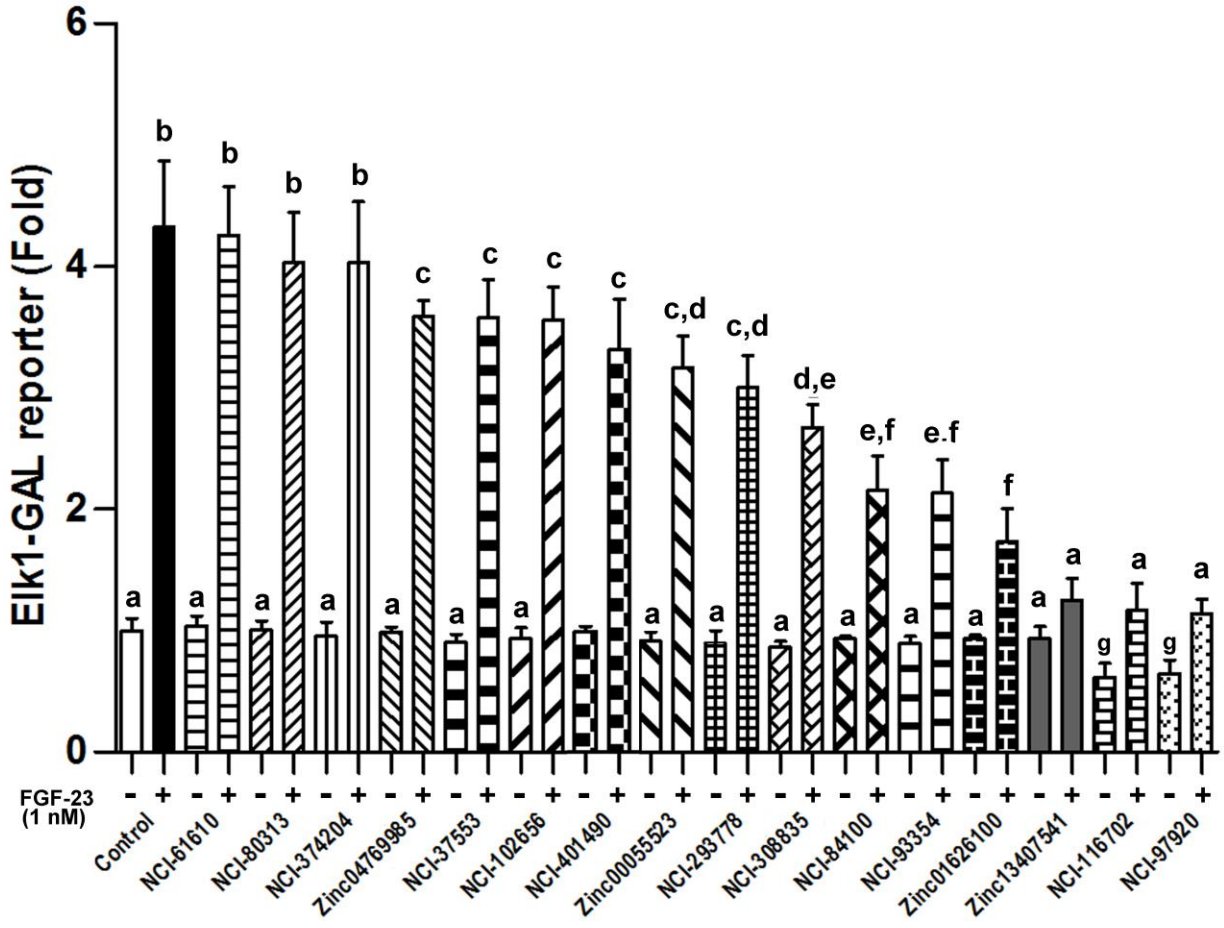

Fig. 3. Effects of 16 chemical probes on Gal-Elk1 luciferase reporter activities in the absence and presence of rFGF-23. Data are expressed as the mean ± S.D. from three independent experiments. Values sharing the same superscript in different groups are not significantly different at $P<0.05$.

Dose-dependent response of chemical probes in antagonizing FGF-23 signaling

To further explore the inhibitory effects of the four most potent chemical probes, we performed additional studies using doses ranging from 10^{-9} to 10^{-5} M. We observed that all four probes exhibited dose-dependent inhibition of FGF-23 signaling (**Fig 4**). The estimated IC_{50} values for Zinc13407541, NCI_97920, NCI_116702, and Zinc01626100 were 0.45±0.24, 1.11±0.22,

1.14±0.24 μM, and 4.57±0.22 μM, respectively (**Fig 4, A to D**). Next, we evaluated the potential

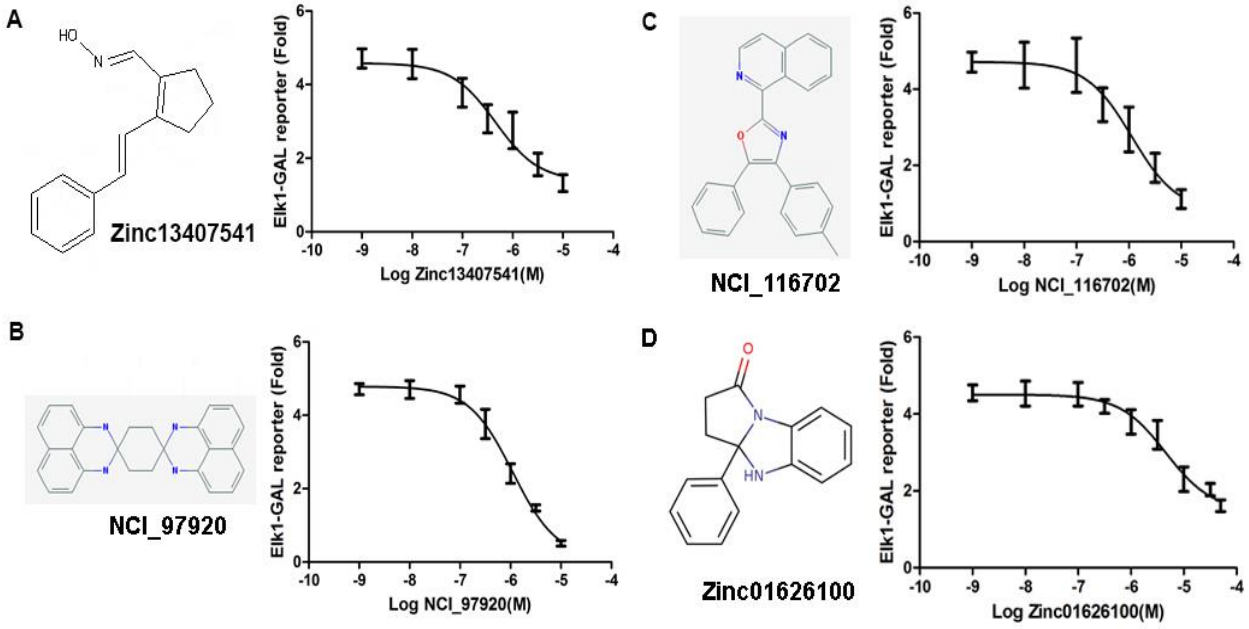

Fig. 4. Molecular structure and dose-response curves of 4 novel FGF-23 antagonists. (**A**) Zinc13407541; (**B**) NCI_97920; (**C**) NCI_116702; (**D**) Zinc01626100.

druggability of each of the platforms using various drug-likeness filters (www.chemicalize.org) as previously described (*61-67*). In general, each of the platforms exhibited drug-likeness with ZINC13407541 and ZINC01626100 having the most drug-like features.

Multicenter Ensemble Docking To Identify Possible Binding Sites for FGF-23 Antagonists

To better understand the structural basis for antagonist binding and to select compounds for additional testing, we performed additional docking using the two best candidate probes, Zinc13407541 and Zinc01626100. As protein flexibility is an important factor in ligand binding (*68-70*), these docking calculations were refined by subjecting the protein to MD simulations with the backbone unrestrained, thus permitting more complete exploration of structural fluctuations than in the original virtual screen.

Zinc13407541 and Zinc01626100 were docked to the potential binding centers identified in the multiple conformers of the protein (See **Materials and Methods**)(**Fig. 5**). Briefly, the conformers were derived from clustering the molecular dynamics trajectories and the binding centers were identified by FTMap. The docking calculations were not sufficiently accurate to identify unambiguous high-precision 3D structures of the two compounds complexed with the protein. Nev-

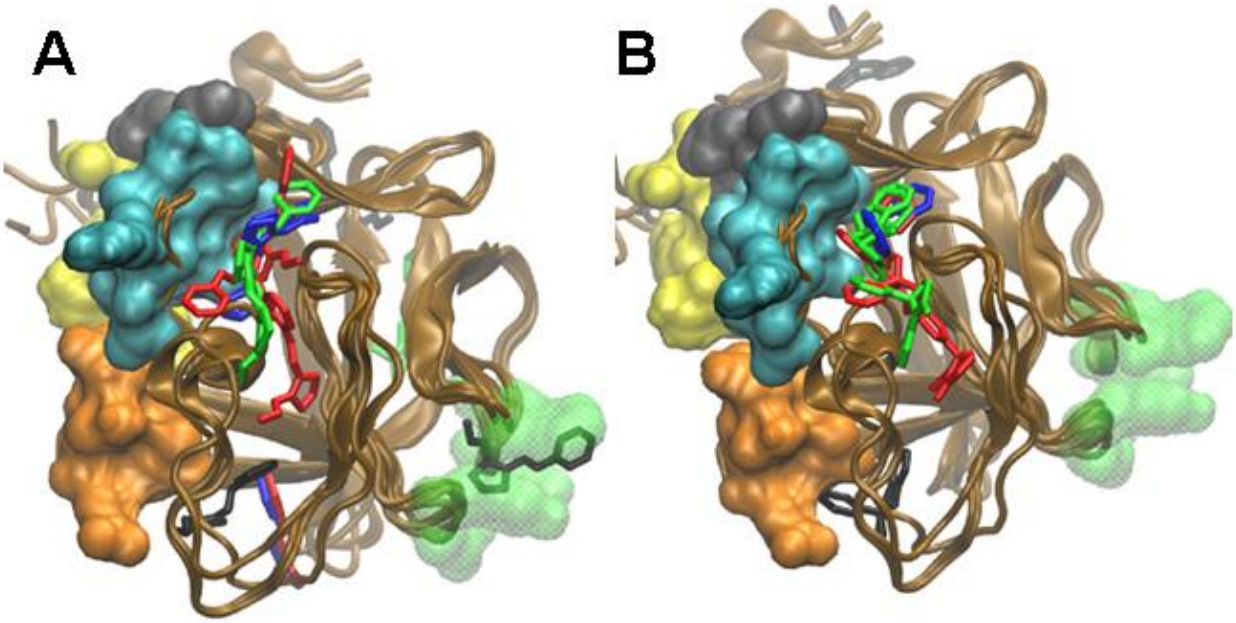

Fig. 5. The results of the multicenter ensemble docking of Zinc13407541 and Zinc01626100. (**A**) Best scored poses of the docking of Zinc13407541. (**B**) Best scored poses of docking of Zinc1626100. The binding epitopes identified by Ref (2) are colored in cyan, gray, orange, and yellow.

ertheless, insight can be gained by examining the highest-scoring poses. Docking poses found within error of the highest-scoring position are shown in **Fig. 5**. In most of these poses the ligands bind in areas predicted, from alignment with a crystal structure of FGF-2 bound to FGFR1, to be critical for the formation of the FGF-23:FGFR1 complex(*8*).

Zinc13407541 poses mostly form multiple hydrogen bonds, with various of the side chains of Asn112, Gln131, Tyr132, Glu111, Leu138 and Arg140 (**Fig. 6A to 6H**), consistent with the

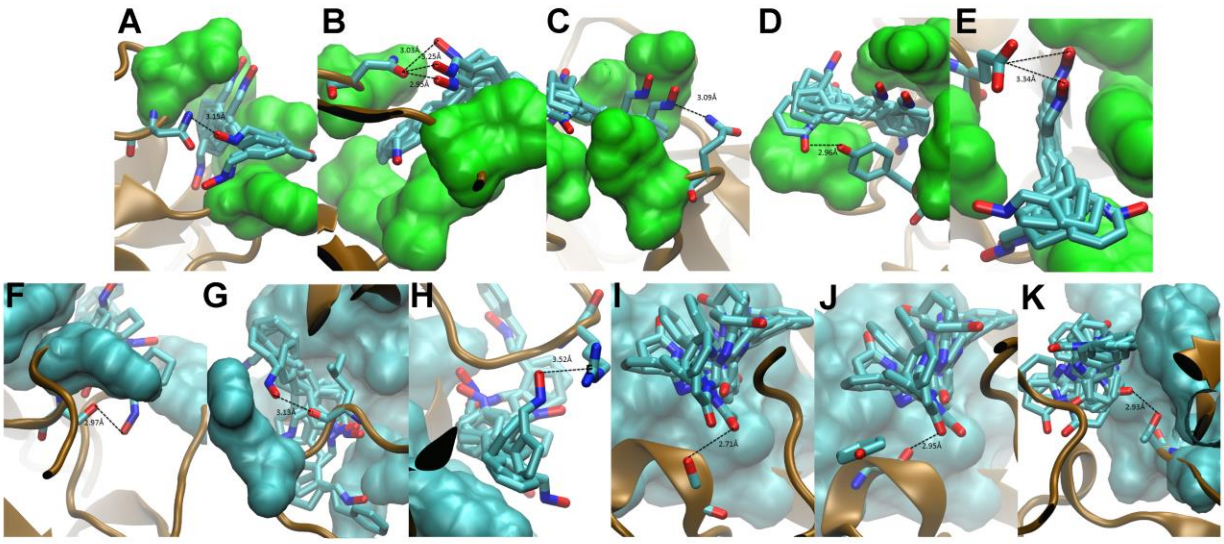

Fig. 6. Predicted intermolecular interactions between the N-terminal FGF-23 and the antagonist compounds. Zinc13407541 interacts with the Asn112 (**A** and **B**), Gln131 (**C**), Tyr132 (**D**), Glu111 (**E**), Ser155 (**F**), Leu138 (**G**), and Arg140 (**H**). Both Zinc13407541 and Zinc 01626100 form hydrogen bonds with the side chain of Ser155 (I). Zinc01626100 also interacts with the backbone oxygen of Tyr154 (**J**) and the side chain of Thr44 (**K**).

ability of lower concentrations of this compound to inhibit FGF-23 function (**Fig. 4A**). Arg140 is of particular note because it forms interactions with the ligand in the FGF-23 crystal structure (*53*) (**Fig. 6H**). Both Zinc13407541 and Zinc 01626100 form hydrogen bonds with Ser155 in the pre viously-predicted FGF1 binding region (*8*) (**Fig. 6I**). Zinc01626100 also forms hydrogen bonding interactions with the backbone oxygen of Tyr154 and the side chain of Thr44 (**Fig 6, J and K**). Based on dose response in Fig 4 and further modeling in Fig 5 and 6, we selected Zinc13407541 for testing target engagement and functional response *in vitro* and *in vivo*.

Effects of Zinc13407541 on FGF23/FGFR1-α-Klotho complex formation and FGF-23 thermal stability

To assess engagement between Zinc13407541 and FGF-23, we performed co-immunoprecipitation and protein thermal shift assays. We performed co-immunoprecipitation assays us-

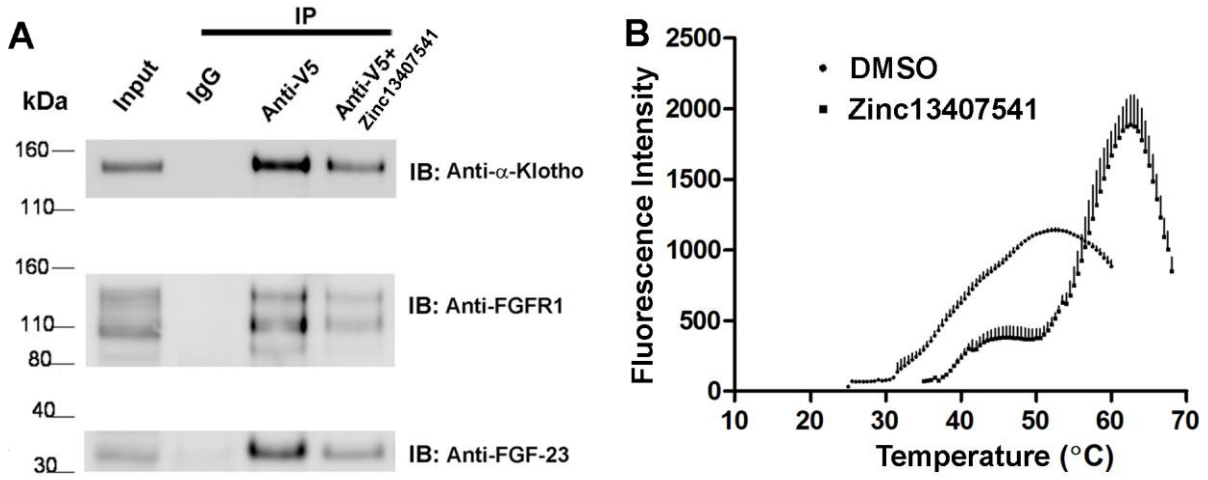

Fig 7. Target engagement assays of FGF-23 antagonist (Zinc13407541) and FGF-23 protein. (**A**) Co-immunoprecipitation (Co-IP) assay; (**B**) Protein thermal shift assay. Data are expressed as the mean ± S.D. from three independent experiments.

ing HEK-293T cells co-transfected with V5-tagged FGF-23, full-length FGFR1, and membrane α-Klotho in the absence and presence of Zinc13407541. We found that the anti-V5 antibody co-precipitated α-Klotho, FGFR1 and FGF-23, indicating that these three factors form a complex. Addition of Zinc13407541 (10 μM) markedly disrupted FGF-23 and FGFR1/α-Klotho complex formation (**Fig 7A**), indicating that Zinc13407541 inhibits FGF-23/FGFR1-α-Klotho complex interaction. We confirmed target engagement by protein thermal shift assays. Using Sypro orange to monitor FGF-23 thermal unfolding, we found that Zinc13407541 (200 μM) stabilized 5 nM of FGF-23, resulting in a 16.5°C shift in melt temperature (Tm) (**Fig 7 B**).

Specificity of Zinc13407541 to antagonize FGF-23.

To test the specificity and selectivity of Zinc13407541 requires examining FGFR activation

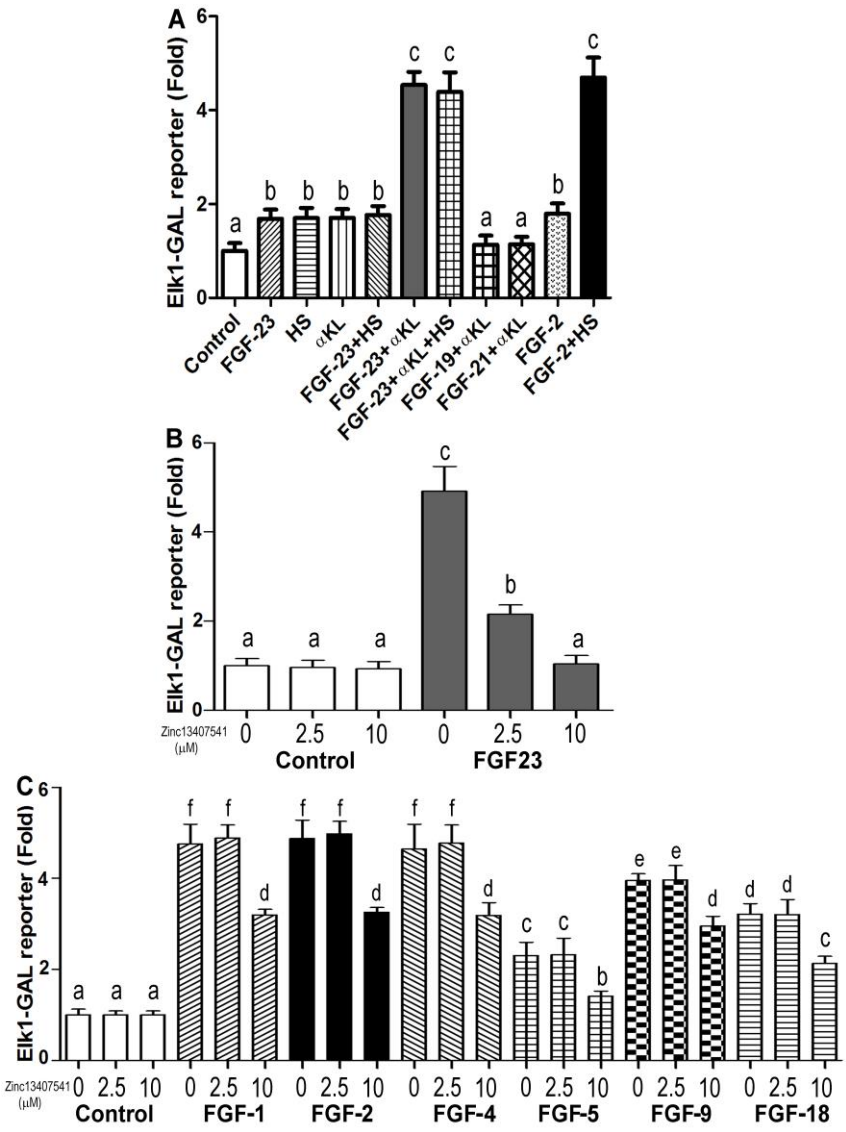

by other FGFs in the presence of co-factors required for optimal ligand-dependent FGFR activation. We examined the ability of 9 different FGF ligands from 6 FGF subfamilies to activate endogenous FGFRs in HEK-293 cells overexpressing α-Klotho signaling or in cells lacking α-Klotho but treated with HS, the co-factor for paracrine FGF activation of FGFRs (**Fig 8)**. We found that FGF-23 in the presence of α-KL markedly stimulated

Fig. 8. Effects of different dose of FGF-23 antagonist Zinc13407541 on Gal-Elk1 luciferase reporter activities in the absence and presence of FGF ligands from different FGF subfamilies. (**A**) FGF-23 activation of FGFR/α-KL receptor complex in the presence of α-KL and FGF-2 activation of classical HS-dependent FGFR signaling in the absence of α-KL; (**B**) Dose-dependent inhibition of α-KL dependent signaling by Zinc13407541. Partial inhibition occurs at concentration of 2.5 μM, and complete inhibition occurs at concentration of 10 μM; (C) Dose-dependent inhibition of HS-dependent FGFR signaling by Zinc13407541. Partial inhibition occurs only at concentration of 10 μM. All ligands were tested at concentrations of 1 nM. Data are expressed as the mean ± S.D. from three independent experiments. Values sharing the same superscript in different groups are not significantly different at $P<0.05$.

Elk1-Gal reporter activity, whereas in the absence of α-KL the response was minimal (**Fig 8A**). In contrast, expression of α-KL did not impart FGFR activation to either FGF-19 or FGF-21, hormonal FGFs that require β-Klotho. In addition, Heparan sulfate (HS), which is the cofactor for paracrine FGF ligands, did not support FGF-23 activation of FGFRs. Using FGF2 as a prototypic paracrine FGF ligand; we demonstrated that HS augmented FGF2 activation of FGFR in HEK-293 cells (**Fig 8A**).

Zinc13407541 resulted in a dose-dependent inhibition of FGF-23 activation of FGFR/α-KL receptor complex. A significant ~60% and 100% inhibition of FGF-23 stimulation of Elk1-Gal reporter activity were observed at concentrations of 2.5 and 10 μM, respectively (**Fig 8B**). We also tested the effects of Zinc13407541 to inhibit FGF 1, 2, 4, 5, 9, and 18 action of HS-dependent FGFR signaling. Zinc13407541 at concentrations of 2.5 μM did not inhibit FGFR activation of these FGF ligands; however, Zinc13407541 at concentrations of 10 μM reduced FGFR activation by ~ 30% (**Fig 8C**). These findings suggest that lower doses of Zinc13407541 selectively inhibit FGF-23 mediated FGFR/α-KL signaling, whereas higher doses display partial and non-specific inhibition of non-hormonal FGF ligand activation of FGFR/HS signaling.

Effects of Zinc13407541 on FGF-23 regulation of gene expression in primary renal tubule cell cultures

The kidney is a physiologically important target for FGF-23. Next, we tested the effects of Zinc13407541 blocking FGF-23 effects on primary renal tubule cell cultures. We found that primary tubule cells expressed FGFR1/α-Klotho complexes and responded to exogenous FGF-23 exposure by increased ERK activity. The FGF-23 inhibitor Zinc13407541 had no effect on the expression of the FGFR1/α-Klotho complex (**Fig 9A**), but significantly attenuated FGF-23-mediated ERK activation in these tubules (**Fig 9B**). To examine physiological effects of this hormone, we assessed the effects of rFGF-23 on cytochrome P450 family 27 subfamily B member 1

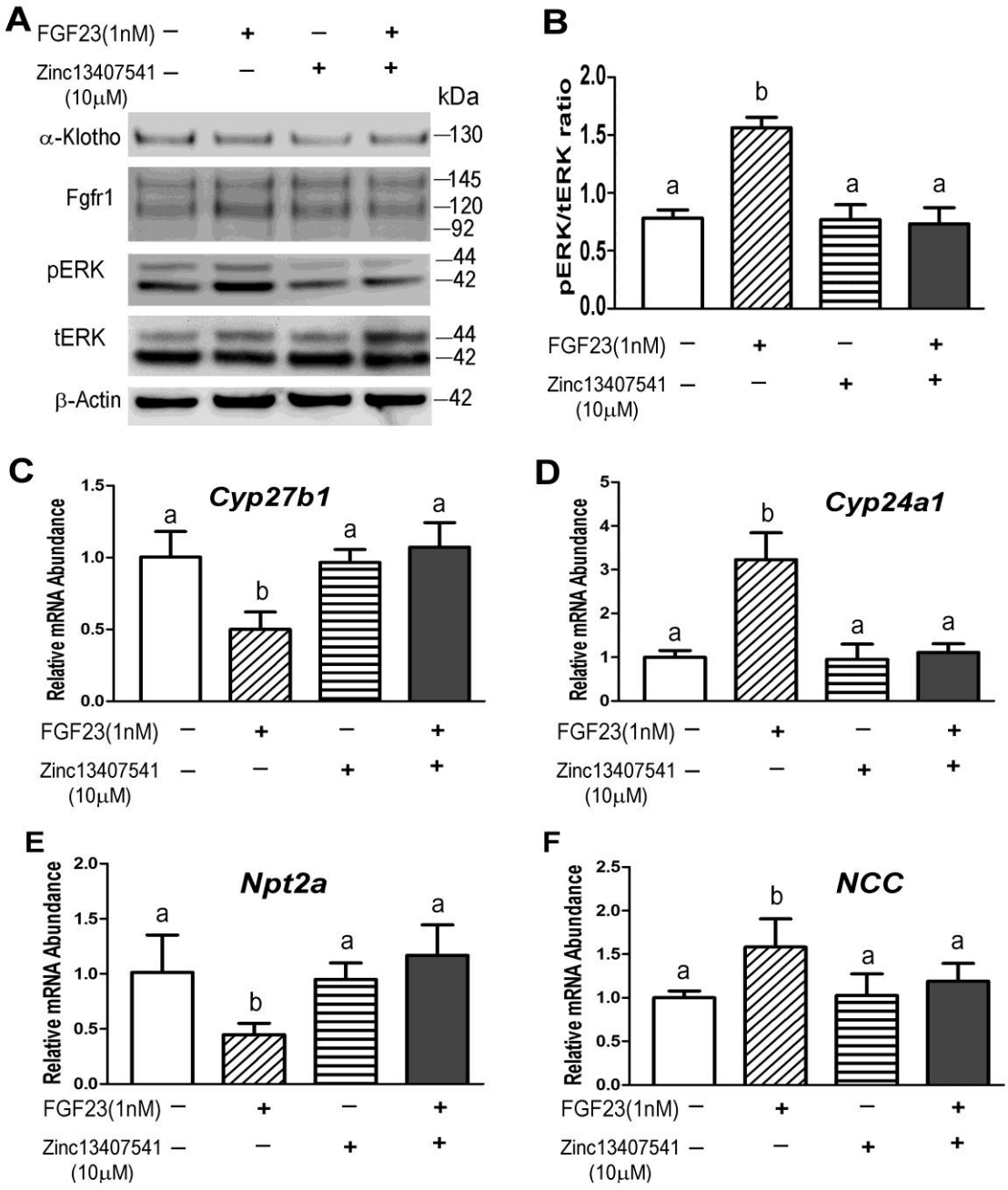

Fig. 9. The effects of the FGF-23 antagonist (Zinc13407541) on FGF23-induced signaling in primary tubule cell cultures. (**A**) Western blot analysis of FGFR1/α-Klotho signaling; (**B**) Quantification of the pERK/tERK ratios; (**C-F**) Quantitative real-time RT-PCR analysis of total *Cyp27b1*, *Cyp24a1*, *Npt2a*, and *NCC* transcripts. Data are expressed as the mean ± S.D. from three independent experiments. Values sharing the same superscript in different groups are not significantly different at $P<0.05$.

(*Cyp27b1*), cytochrome P450 family 24 subfamily A member 1 (*Cyp24a1*), type IIa Na^+-dependent

phosphate co-transporter (*Npt2a*), and thiazide-sensitive Na^+-Cl^- cotransporter (*NCC*) expression in isolated tubule cells. Consistent with known actions of FGF-23, rFGF-23 inhibited *Cyp27b1*, and *Npt2a* expression and stimulated *Cyp24a1* and *NCC* message expression in isolated renal tubules. Treatment with Zinc13407541 (10μM) inhibited FGF-23 regulation of *Cyp27b1*, *Cyp24*a1, *Npt2a*, and *NCC* expression in primary tubule cell cultures (**Fig 9C to 9F**).

Therapeutic effects of FGF-23 antagonist (Zinc13407541) on homozygous *Dmp1* knockout mice *in vivo*, a murine model of FGF-23 excess

Finally, to evaluate therapeutic potential of Zinc13407541, we examined its effect to block the biological effects of excess FGF-23 in both wild type and *Dmp1* knockout mice. Eight-week-old wild type and homozygous *Dmp1* knockout mice treated with IP injection of Zinc13407541 (100 mg/kg) twice a day for three days sur-

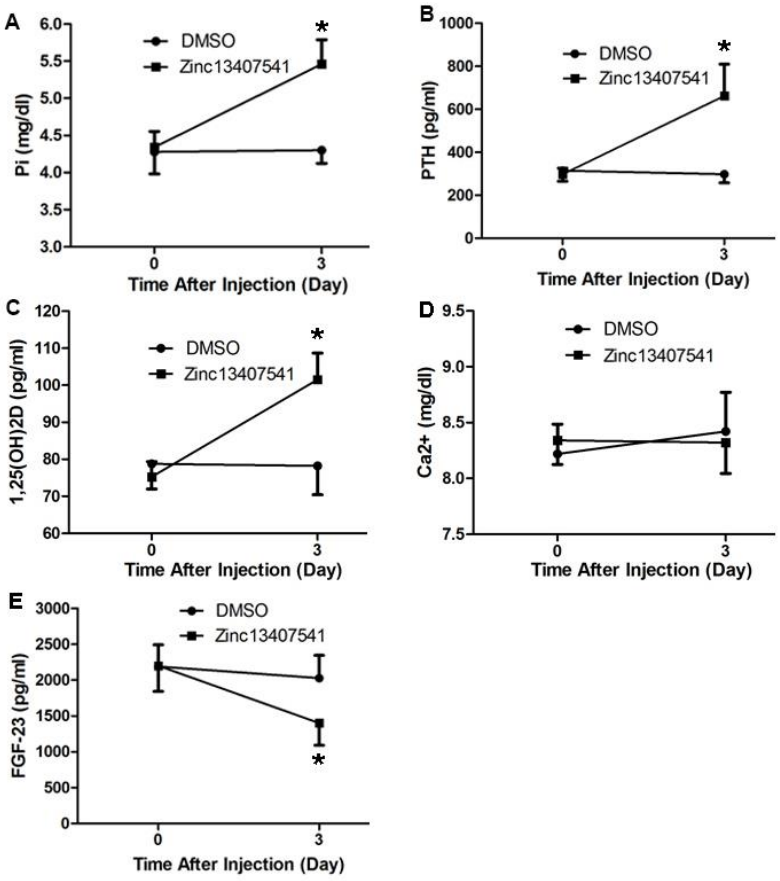

Fig 10. The improvement of hypophosphatemia, PTH, and 1,25(OH)$_2$D3 metabolism after 3 days of FGF-23 antagonist (Zinc13407541) injection in the homozygous *Dmp1* knockout mice. Serum biochemical analyses of phosphate (Pi) (**A**); PTH (**B**); 1,25(OH)$_2$D3 (**C**); calcium (Ca^{2+}) (**D**); and FGF-23 (**E**); Data are expressed as the mean ± S.D. from 4-5 serum samples of 8-week-old mice.* indicates significant difference from vehicle (DMSO) control mice.

vived, no toxic and lethal effects were observed. As previously reported (*71, 72*), we observed that the *Dmp1* knockout mice exhibited hypophosphatemia and suppressed 1,25$(OH)_2$D associated with increased serum FGF-23. Compared to vehicle (5% DMSO in PBS solution) Zinc13407541 (100 mg/kg) administered by intraperitoneal injection twice a day for three days to *Dmp1* null mice resulted in a significant increase in serum phosphate levels, PTH, and 1,25(OH)2D levels (**Fig 10, A-C**), but no changes in serum calcium concentrations (**Fig 10D**). Unexpectedly, treatment with Zinc13407541 in *Dmp1* null mice also significantly decreased serum FGF-23 levels by approximately 35% (**Fig 10E**). In addition, we obtained the similar results in changes of serum phosphate, calcium, PTH, and 1,25(OH)2D levels in the wild type mice treated with Zinc13407541 (100 mg/kg) (**Fig S1, A-D**). However, we found that the serum FGF-23 levels remain normal in wild type mice treated with Zinc13407541 (**Fig S1, E**).

DISCUSSION

Using homology modeling, molecular dynamics simulation and virtual high throughput screening to guide experiment, we have identified, for the first time, novel small molecules that interact with the FGF-23 ligand to block its activation of the FGFR1/α-Klotho receptor complex. These molecules, by targeting the FGF-23 ligand, differ from other small molecules that inhibit FGFR activation by binding to the extracellular domain of the FGFR or its internal tyrosine kinase domain (*49-51, 73, 74*). The success of the structure-based computational approach is notable, since no *a priori* mutagenesis or other experimental data guided the docking calculations. This validates the utility of the molecular dynamic simulations to overcome limitations of interpreting docking results using a static protein target (*75*). Specifically, our computational strategy generated homology models with different initial configurations of the backbone that were refined by constrained MD simulations. Using these refined structures for *in-silico* virtual screens identified 16 compounds predicted to bind to FGF-23. Experimental testing of these 16 compounds identified four that strongly disrupted FGF-23 activity. These compounds had no previously known biological functions. Thus, we have shown that our virtual high-throughput screening approach can successfully identify novel chemical probes for specific targets, complementing other recent successes using the same approach (*76*).

Of the compounds identified, Zinc13407541 and Zinc01626100 appear to be the best potential candidates for further lead development and pre-clinical testing. These two compounds are structurally unrelated. Zinc13407541, or N-[[2-(2-phenylethenyl)cyclopenten-1-yl]methylidene]hydroxylamine, has a molecular formula of $C_{14}H_{15}NO$ and molecular weight of 213. Zinc01626100, or 6-phenyl-2,7-diazatricyclo[6.4.0.$0^{2,6}$]dodeca-1(12),8,10-trien-3-one, has a molecular formula of $C_{16}H_{14}N_2O$ and molecular weight of 250. Based on estimated IC_{50} values of functional assays and differences in binding to primary and secondary pockets of FGF-23, compound Zinc13407541 is predicted to exhibit more than 10-fold higher affinity than compound Zinc01626100. In addition,

compound Zinc13407541 shows preferential and complete inhibition of FGF-23 action of FGFR/α-Klotho signaling in a heterologous cell model, although it exhibited partial inhibitory effects on several other FGF family members tested at higher concentration.

To probe in detail the specific sites of binding for the experimentally verified compounds we performed unconstrained MD simulations and ensemble docking, which incorporates the idea of an ensemble of possible binding locations as well as conformations of the antagonist compounds. The results suggest the antagonists bind to a region that is predicted to form protein-protein interactions with FGFR1. Our target engagement assays confirmed that Zinc13407541 directly binds to FGF-23 proteins and inhibits FGF-23-FGFR1-α-Klotho complex interaction. Further computational modeling and medicinal chemistry are needed to define structure activity/function relationships around these probes to demonstrate feasibility of extensive lead optimization and developing compounds with greater specificity. Also, as the computations identified residues that may be important to antagonist binding, mutagenesis and additional target engagement studies will be able to confirm these binding sites (*51, 73, 74*).

To our knowledge, these are the first small molecules to be identified that inhibit FGF-23 activation of FGFR/α-KL complexes through targeting the ligand to disrupt receptor interactions and activation. Both thermal shift assays and immunoprecipitation studies confirm the effects of Zinc13407541 to bind to FGF-23 and disrupt its interaction with FGFR/α-Klotho complex; and studies in heterologous cell-reporter models show dose-dependent effects of Zinc13407541 to inhibit FGF-23 activation of FGFR/α-Klotho signaling. Zinc13407541 provides greater selectivity than the currently available receptor tyrosine kinase inhibitors that are used to inhibit all of FGFs-FGFR signaling (*77, 78*). Further, we show the biological relevance of these observations, by the additional findings that Zinc13407541 inhibits FGF-23 regulation of *Cyp27b1*, *Cyp24*a1, Npt2a, and NCC expressions in primary tubule cell cultures. Consistent with Zinc13407541 inhibition of

FGF23-regulated *Cyp27b1* and *Cyp24a1* expressions in renal tubule cells, Zinc13407541 administration to *Dmp1* null mice also raised serum $1,25(OH)_2D3$ levels. More importantly, Zinc13407541 administration improved hypophosphatemia in the *Dmp1* null mouse model of FGF-23 excess. These data indicate that Zinc13407541 may have clinical utility to block FGF-23 effects on the kidney.

Similar to our findings, a recombinant human IgG1 monoclonal antibody, KRN23, that binds to FGF-23 has been shown to correct hypophosphatemia and abnormalities in vitamin D metabolism in both mouse homologue models and humans with XLH (*79*). Interestingly, Zinc13407541 treatment also increased circulating PTH levels in *Dmp1* null mice without altering serum calcium concentrations. This response is consistent with inhibition of FGF-23 effects to activate FGFR1/α-Kl in the parathyroid gland and suppress PTH secretion (*21*), but differs from effects of FGFR inhibitor and anti-FGF-23 antibody treatments, which suppressed serum PTH levels in the *Hyp* mouse model of FGF-23 excess (*78, 80*). There are other notable differences between Zinc13407541 and KRN23 as potential therapeutics. KRN23 requires parenteral administration and has a long-half life that limits dose titrations. Since over-suppression of FGF-23 leads to tumoral calcinosis, use of KRN23 may have a narrow therapeutic window compared to an orally administered small molecule FGF-23 antagonist. These small molecule drug antagonists identified herein also provide an important alternative to the biological molecules that are currently under development to inhibit FGF-23 actions.

While Zinc13407541 is a platform for targeting the FGF-23 ligand, additional modifications will likely be needed to realize its therapeutic potential. Indeed, at high concentrations it also blocks other FGF ligands that lack the unique FGF-23 C-terminus that interacts with α-Klotho. Other approaches to more selectively inhibit FGF-23 activity may be achieved by blocking interactions between the FGF-23 C-terminus and α-KL (*11*). For example, an unstructured 26-residue

sequence of the C-terminal domain was discovered to bind the FGFR1/α-KL complex (*52*), leading to competitive inhibition of FGF-23 activation of the FGF receptor (*81*). Additional modeling may identify new chemical antagonists that target both the N- and C- termini of FGF-23 that would likely impart greater efficacy and specificity in disrupting FGF/α-Klotho signaling. Nevertheless, the discovery of chemical compounds that antagonize FGF-23 activation of FGFRs sets the stage for ultimately developing clinical drug candidates to treat disorders of FGF-23 excess.

In conclusion, we validate the utility of a computationally driven structure-based drug discovery approach employing homology modeling, molecular dynamics (MD) simulations and docking to identify novel small-molecules that inhibit FGF-23 activation in the presence of FGFR1 and α-KL. These chemical probes provide a new way to inhibit ligand-FGFR1-α-KL interactions and FGFR signaling inhibition without targeting the intrinsic tyrosine kinase activity and identify a chemical platform on which to develop lead compounds as potential treatments for disorders caused by FGF-23 excess. There are 22 mammalian FGFs and four alternative spliced FGF receptor genes (FGFR1-FGFR4) that encode seven membrane-associated tyrosine kinase isoforms (FGFRs 1 b, 1c, 2b, 2c, 3b, 3c and 4). An analogous approach might be used to disrupt other FGF ligand and FGFR interactions, thereby establishing a new paradigm for developing drugs that selectively disrupt FGFR activation by each of these FGF ligands.

MATERIALS AND METHODS

In-silico virtual screening for the identification of trial compounds

Four computational models of FGF-23 were prepared using an FGF-23 crystal structure (PDBID: 2p39) (*53*) and three homology models generated with the aid of the Max Planck Bioinformatics Toolkit (*82*). An HHPred sequence search (*83*) resulted in the selection of three crystal structures, two of FGF19 (PDBIDs: 1pwa (*84*) and 2p23 (*53*)) and one of FGF12 (PDBID: 1q1u (*85*), to be used as templates to build the homology models. The structures for the three homology models were constructed with Modeller (*86*) by threading the FGF-23 sequence along the corresponding backbone geometry. The fourth model is based on the FGF-23 crystal structure (PDBID: 2P39 (*53*)). The heparin analogue and crystal-resolved solvent were removed from the crystal structure in preparation for short, constrained MD simulations.

All four models were prepared and simulated using CHARMM-GUI (*87*) and CHARMM (*88*). The proteins were protonated using the HBUILD facility of CHARMM (*89*), and each model was solvated in an octahedral unit cell (a=b=c=85 Å). The structures were energy minimized for 500 steps of steepest descent (*90*) and 500 steps Adopted Basis Newton-Raphson (ABNR) (*91*) with the backbone and side chains restrained using 1.0 and 0.1 kcal mol^{-1}*$Å^{-2}$ harmonic potentials, respectively. Using the same restraints on the solute, the solvent was relaxed using molecular dynamics (MD) with the NVE ensemble for 200 ps with a 1 fs timestep. For production MD simulations, the same harmonic restraint was used to constrain the backbone while the side chains were unrestrained. The SHAKE (*92*) algorithm was also used to constrain all bonds including hydrogen in the MD steps for solvent relaxation and the production simulations. The MD simulations were carried out using the NPT ensemble at 1 atmosphere and 298 K with a 2 fs timestep. Eight independent seeds were carried out for each homology model; each seed was run with 2 fs time steps for 7 ns. Short MD simulations with the backbone constrained to the neighborhood of

the initial starting structure have been shown to be adequate for the refinement of homology models (*93*).

The final configuration of each seed of each homology model was submitted to the FTMAP web server (*94*) to identify possible binding sites. FTMap has been shown to be adept at identifying druggable hotspots in proteins, particularly when used in conjunction with ensemble docking as in the present work (*94-96*). The consensus clusters generated by FTMAP were culled to binding centers (at least 7.5 Å apart) using K-means clustering and HackaMol (*97*). The NCI Diversity Set 2 was used to carry out initial screens for each refined homology model. Subsequently, the ZINC database (*98*) was screened for molecules with a Tanimoto cutoff (*99*) of 0.8. This was done to ensure that the molecules screened from the ZINC database were chemically unique from those of the NCI Diversity Set 2. Open Babel (*100*) was used to build the starting configuration of each molecule from the respective SMILES representation (*101*). MGL tools (*102*) was used to generate the PDBQT for each candidate small molecule (ligand) and each FGF-23 configuration (receptor). The HackaMol interface to Autodock-Vina (*103*) was used for all screens. A 20Å cubic screening box, centered at the clustered potential binding sites identified by FTMap was used for each docking run. The Autodock Vina exhaustiveness parameter was set to 24.

Chemicals and reagents

The most promising molecules from each virtual screen were tested experimentally. Four of the compounds [ZINC13407541, ZINC00055523, ZINC04769985, and ZINC01626100] were purchased from AKos Consulting & Solutions Deutschland GmbH (Austr. 26 D-79585 Steinen, Germany). We obtained 12 chemicals [NCI_293778, NCI_37553, NCI_308835, NCI_84100_a, NCI_61610, NCI_80313, NCI_116702, NCI_97920, NCI_93354_a, NCI_374204 (ZINC01589294), NCI_401490 (ZINC01594155), and NCI_102656 (ZINC01674794)] from the

Developmental Therapeutic Program of the National Cancer Institute (Rockville, MD, USA). Recombinant human FGF-23 and FGF-2 were purchased from R&D Systems (Minneapolis, MN, USA). Synthetic human C-terminal FGF-23 (residues 180-251) peptide (FGF-23C) was obtained from Phoenix Pharmaceuticals, Inc. (Burlingame, CA, USA). Recombinant human FGF-1, FGF-4, FGF-5, FGF-9, FGF-10, FGF-18, FGF-19, and FGF-21 were purchased from PeproTech (Rocky Hill, NJ, USA). The laboratory of Dr. Jesse D. Carrick also synthesized compound ZINC13407541 at Tennessee Technological University for *in vivo* animal experiments. The NMR Spectra analysis showed that the purity of ZINC13407541 was more than 95%.

Cell culture and in vitro screening assays

For FGF-23-mediated activation of FGFR1/α-KL complex, HEK-293 cells were transiently transfected with either empty expression vector or full-length human α-KL along with the Gal-Elk1 luciferase reporter system (*11*) and *Renilla* luciferase-null as internal control plasmid. Transfections were performed by electroporation using Cell Line Nucleofector Kit R according to the manufacturer's protocol (Amaxa, Inc., Gaithersburg, MD). Thirty-six hours after transfection, the transfected cells were treated with the test compound in the presence or absence of 1 nM FGF-23. After 5 hours, the cells were lysed and luciferase activities measured using a Synergy H4 Hybrid Multi-Mode Microplate Reader (Winooski, VT, USA) and Promega Dual-Luciferase Reporter Assay System (Madison, WI, USA).

Primary tubule cell cultures, western blot, and quantitative real-time RT-PCR

The animal protocols and procedures have been approved by Institutional Animal Care and Use Committee of the University of Tennessee Health Science Center (IACUC ID: 15-138.0).

Wild-type C57BL/6 mice at age of 12–16 weeks were used in the current experiments. The isolation of tubular cells was performed as described by Weinman *et al.* (2011) with some modifications (*104*). Briefly, kidney cortices were decapsulated and dissected in order to obtain 1 mm^3 fragments. The fragments were then digested in 10 mL of Hanks Balanced Salt Solution (HBSS) (Invitrogen Corp., Carlsbad, CA) with 1% Worthington collagenase type II (200 units/mL) and 0.025% soybean trypsin inhibitor. This step was performed three times at 37°C for 15 minutes, and the suspension was filtered through filters with a mesh size of 100 µm after each digestion. The cell suspension was washed twice in PBS (Phosphate Buffered Saline) and centrifuged for 5 minutes at 200 g. Cells were cultured in Matrigel-coated 6-well plates with complete DMEM/F12 1:1 medium containing 10 ng/mL EGF, 1% penicillin/streptomycin, 1% L-glutamine, 15 mM HEPES, 40 ng/mL (0.11 mM) hydrocortisone hydrocortisone, insulin/transferrin/selenium (Invitrogen, 5 mg/mL, 2.75 mg/mL and 3.35 ng/mL respectively) at 37°C under 5% CO_2 in a humidified atmosphere. The culture medium was changed after 24 hours in order to eliminate non-adherent cells and residual cellular fragments. The tubule cells were grown in the growth medium for 4 days and treated with FGF-23 and the FGF-23 inhibitor for 4 hours. The western blot and quantitative real-time RT-PCR were performed as previously described (*105*). Anti-FGFR1 (D8E4, #9740), Anti-Phospho-ERK1/2 (Thr202/Tyr204) (D13.14.4E, #4370), and Anti-ERK1/2 (#9102) were purchased from Cell Signaling Technologies (Danvers, MA). Anti-Klotho (KAL-KO604) was purchased from Cosmo Bio USA, Inc. (Carlsbad, CA). Anti-β-actin (sc-47778) antibody was obtained from Santa Cruz Biotechnology (Paso Robles, CA). The intensity of bands was quantified using Image J software (http://rsb.info.nih.gov/ij/).

Ensemble Docking of experimentally verified hits on the N-terminal domain of FGF-23

In order to probe in more detail possible binding modes of the two lead compounds, unconstrained simulations of the target were performed. These additional MD simulations were carried out the with Amber suite of programs (*106*). The 2P39 crystal structure was used as the starting structure for these simulations (*53*). The system was solvated with an octahedral, periodic box consisting of 6,810 TIP3P water molecules and 3 Cl^- atoms were added to maintain electrostatic neutrality of the system. Here, the crystallographic water molecules were retained. The protein topology file was built with the parm99SB (*107*) version of the Cornell force field (*108*). The system was energy minimized via a two-step process. First, FGF-23 was held fixed with a force constant of 500 kcal*mol^{-1}*$Å^{-1}$ while the system was minimized with 500 steps of steepest descent (*90*) performed followed by 500 steps of conjugate gradient method (*109*). In the second minimization step, the restraint on FGF-23 was removed and 1000 steps of steepest decent were performed followed by 1500 steps of conjugate gradient. The system was heated to 300K while holding the protein fixed with a force constant of 10 kcal*mol^{-1}*$Å^{-1}$ while running 1000 MD steps. Then the restraints were released and 1000 MD steps were run. The SHAKE (*92*) algorithm was used to constrain all bonds involving hydrogen in the simulations as in the in-silico virtual screen. A 200 ns MD run was completed from a randomly generated seed. A snapshot from the trajectory was written every 1,000 MD steps. This yielded a total of 100,000 snapshots for further analysis.

These MD trajectories were analyzed with cluster analysis as implemented in the ptraj software in Amber12 (*110*). The cluster analysis resulted in the identification of 36 clusters. One representative structure from each cluster was used to create a small ensemble of structures for docking of the experimentally verified antagonist compounds. From this small ensemble, four structures were randomly selected for binding site identification and docking of the experimentally verified FGF-23 inhibitors with Autodock-Vina (*103*). FTMap was used to identify potential binding sites for the inhibitor compounds (*111, 112*). The experimentally identified chemical probes were then docked to each binding site identified by FTMap. To identify locations where the inhibitors bind FGF-23's N-terminal domain, all the centers identified by FTMap were used to probe a larger

portion of the protein surface along with a large search box size. Zinc13407541 and Zinc01626100 were docked to each potential binding center on each of the four randomly selected structures from the ensemble of structures created from the MD simulations. This is in contrast to other studies where only the top five consensus clusters are used for drug design (*113*). A 20x20x20 search box was used and the exhaustiveness parameter was set to 25. The binding site centers were not combined in an effort to allow the docking simulations to search a larger part of the protein surface for stable binding locations.

Target engagement assays

We performed co-immunoprecipitation (Co-IP) assays using HEK-293T cells co-transfected with V5-tagged FGF-23 (2.0 µg), full-length FGFR1 (2.0 µg), and membrane α-Klotho (µg) in the absence and presence of Zinc13407541 (10 µM). The cells were lysed with ice cold 1 x IP lysis buffer (Pierce Biotechnology, Rockford, IL, USA) containing 1 x protease inhibitors. 50 ul of anti-V5 magnetic beads (MBL International Corporation, Woburn, MA, USA) were added into 400 µL of the lysate supernatant in the absence and presence of Zinc13407541 (10 µM). The mixtures were incubated with gentle agitation for 2 hours at 4°C. The mixtures were placed the tube on the magnetic rack for a few seconds, the magnetic beads were washed 3 times with cold Lysis buffer and suspended in 30 µL of Laemmli's sample buffer. 10 µL of the supernatant sample per lane was loaded in a 4-12% Bis-Tris gradient Gels (Invitrogen, Carlsbad, CA) and carried out for electrophoresis and western blot analysis. Anti-α-Klotho rat mAb (KM2076) was purchased from TransGenic Inc. (Chuo-ku, Kobe, Japan). Anti-FGFR1 (D8E4, #9740) was purchased from Cell Signaling Technologies (Danvers, MA, USA). Anti-FGF-23 (MAB2629) was obtained from R&D Systems, Inc. (Minneapolis, MN, USA).

Next, we conducted protein thermal shift assay using a real-time PCR instrument as previously described. 50 µl of solutions consisting of 5 nM FGF-23, 5X Sypro orange, 10 mM HEPES-

NaOH pH 7.5, 150 mM NaCl, and either vehicle DMSO or Zinc13407541 (200 μM) were added to the wells of the 96-well iCycler iQ PCR plate. The plate was heated from 25 to 70 with a heating rate of 0.5 °C/30 seconds. The fluorescence intensity was measured with Excitation/Emission: 490/530 nm.

Animal experiments

All animal research was conducted according to guidelines provided by the National Institutes of Health and the Institute of Laboratory Animal Resources, National Research Council. The University of Tennessee Health Science Center's Animal Care and Use Committee approved all animal studies (Protocol number: 15-138.0). All mice were maintained in our vivarium on a standard diet (7912; Harlan Teklad, Madison, WI, USA). To generate homozygous *Dmp1* knockout mice, we crossed male heterozygous *Dmp1* knockouts with female heterozygous *Dmp1* knockouts to obtain homozygous *Dmp1* knockouts as previously described (*71*). At 8 weeks of age, homozygous *Dmp1* knockout mice were selected to collect blood for serum before treatments. Then the mice were treated with intraperitoneal injection of Zinc13407541 (100 mg/kg) or vehicle control (5% DMSO in PBS solution) twice a day for three days. The serum samples were collected 4 hours after last dose administration. Serum FGF23 levels were measured using the FGF23 ELISA kit (Kainos Laboratories, Tokyo, Japan). Serum phosphorus levels were measured using a Phosphorus Liqui-UV kit (Stanbio Laboratories, Boerne, TX, USA) and serum calcium levels were measured using a Calcium (CPC) Liquicolor kit (Stanbio Laboratories, Boerne, TX, USA). Serum parathyroid hormone (PTH) levels were measured using the Mouse Intact PTH ELISA kit (Immutopics, Carlsbad, CA, USA). Serum 1,25(OH)2D levels were measured using the 1,25-dihydroxy-vitamin D EIA Kit (Immunodiagnostic Systems,Fountain Hills, AZ, USA) as previously described (*105*).

Statistical analysis

We evaluated differences between two groups by unpaired t-test, multiple groups by one-way analysis of variance, and two groups over time by two-way analysis of variance with interactions. All values are expressed as means ± S.D. All computations were performed using a commercial biostatistics software (GraphPad Software Inc. La Jolla, CA).

Acknowledgments

Funding: This work was supported by grant R01-AR045955-15S1 to L. Darryl Quarles from National Institute of Arthritis and Musculoskeletal and Skin Diseases (NIAMS) Building Interdisciplinary Research Team (BIRT) Revision Award. **Author contributions:** Z.S.X., D.R., H.A.V., J.B., and L.D.Q. wrote the manuscript; A.L.C and J.D.C synthesized Zinc13407541; Z.S.X. performed the *in vitro* and *in vivo* experimental studies; D.R., H.A.V., and J.B. performed the computational studies; and C.R.Y., J.C.S., and L.D.Q. guided the research, and reviewed and edited the manuscript. **Competing interests:** The authors declare that they have no competing interests.

REFERENCES AND NOTES

1. N. Itoh, Hormone-like (endocrine) Fgfs: their evolutionary history and roles in development, metabolism, and disease. *Cell Tissue Res* **342**, 1-11 (2010).
2. S. Liu *et al.*, Regulation of fibroblastic growth factor 23 expression but not degradation by PHEX. *J Biol Chem* **278**, 37419-37426 (2003).
3. L. D. Quarles, Evidence for a bone-kidney axis regulating phosphate homeostasis. *Journal of Clinical Investigation* **112**, 642-646 (2003).
4. S. Liu *et al.*, Pathogenic role of Fgf23 in Hyp mice. *American Journal of Physiology - Endocrinology and Metabolism* **291**, E38-E49 (2006).
5. S. Liu *et al.*, Pathogenic role of Fgf23 in Dmp1-null mice. *American Journal of Physiology - Endocrinology and Metabolism* **295**, E254-E261 (2008).
6. L. D. Quarles, The bone and beyond: 'Dem bones' are made for more than walking. *Nature Medicine* **17**, 428-430 (2011).
7. L. D. Quarles, Skeletal secretion of FGF-23 regulates phosphate and vitamin D metabolism. *Nat Rev Endocrinol* **8**, 276-286 (2012).
8. Y. Yamazaki *et al.*, Anti-FGF23 Neutralizing Antibodies Show the Physiological Role and Structural Features of FGF23. *Journal of Bone and Mineral Research* **23**, 1509-1518 (2008).
9. D. M. Ornitz *et al.*, Receptor Specificity of the Fibroblast Growth Factor Family. *Journal of Biological Chemistry* **271**, 15292-15297 (1996).
10. T. Yamashita, M. Yoshioka, N. Itoh, Identification of a novel fibroblast growth factor, FGF-23, preferentially expressed in the ventrolateral thalamic nucleus of the brain. *Biochem Biophys Res Commun* **277**, 494-498 (2000).
11. I. Urakawa *et al.*, Klotho converts canonical FGF receptor into a specific receptor for FGF23. *Nature* **444**, 770-774 (2006).
12. M. Kuro-o *et al.*, Mutation of the mouse klotho gene leads to a syndrome resembling ageing. *Nature* **390**, 45-51 (1997).
13. M. Mitobe *et al.*, Oxidative Stress Decreases Klotho Expression in a Mouse Kidney Cell Line. *Nephron Experimental Nephrology* **101**, e67-e74 (2005).
14. M. C. Hu *et al.*, Klotho: a novel phosphaturic substance acting as an autocrine enzyme in the renal proximal tubule. *The FASEB Journal* **24**, 3438-3450 (2010).
15. I. Z. Ben-Dov *et al.*, The parathyroid is a target organ for FGF23 in rats. *The Journal of Clinical Investigation* **117**, 4003-4008 (2007).
16. L. Zhou, Y. Li, D. Zhou, R. J. Tan, Y. Liu, Loss of Klotho Contributes to Kidney Injury by Derepression of Wnt/β-Catenin Signaling. *Journal of the American Society of Nephrology* **24**, 771-785 (2013).
17. M. Suzuki *et al.*, betaKlotho is required for fibroblast growth factor (FGF) 21 signaling through FGF receptor (FGFR) 1c and FGFR3c. *Mol Endocrinol* **22**, 1006-1014 (2008).
18. T. Shimada *et al.*, Cloning and characterization of FGF23 as a causative factor of tumor-induced osteomalacia. *Proc Natl Acad Sci U S A* **98**, 6500-6505 (2001).
19. K. E. White *et al.*, Autosomal-dominant hypophosphatemic rickets (ADHR) mutations stabilize FGF-23. *Kidney Int* **60**, 2079-2086 (2001).
20. J. Gattineni *et al.*, FGF23 decreases renal NaPi-2a and NaPi-2c expression and induces hypophosphatemia in vivo predominantly via FGF receptor 1. *Am J Physiol Renal Physiol* **297**, F282-291 (2009).
21. O. Andrukhova *et al.*, FGF23 regulates renal sodium handling and blood pressure. *EMBO Mol Med* **6**, 744-759 (2014).

22. B. Dai *et al.*, A comparative transcriptome analysis identifying FGF23 regulated genes in the kidney of a mouse CKD model. *PLoS One* **7**, e44161 (2012).
23. O. Andrukhova *et al.*, FGF23 promotes renal calcium reabsorption through the TRPV5 channel. *EMBO J* **33**, 229-246 (2014).
24. T. Shimada *et al.*, Vitamin D receptor-independent FGF23 actions in regulating phosphate and vitamin D metabolism. *Am J Physiol Renal Physiol* **289**, F1088-1095 (2005).
25. X. Bai, D. Miao, J. Li, D. Goltzman, A. C. Karaplis, Transgenic mice overexpressing human fibroblast growth factor 23 (R176Q) delineate a putative role for parathyroid hormone in renal phosphate wasting disorders. *Endocrinology* **145**, 5269-5279 (2004).
26. T. Larsson *et al.*, Transgenic mice expressing fibroblast growth factor 23 under the control of the alpha1(I) collagen promoter exhibit growth retardation, osteomalacia, and disturbed phosphate homeostasis. *Endocrinology* **145**, 3087-3094 (2004).
27. S. Fukumoto, T. Yamashita, Fibroblast growth factor-23 is the phosphaturic factor in tumor-induced osteomalacia and may be phosphatonin. *Curr Opin Nephrol Hypertens* **11**, 385-389 (2002).
28. I. Z. Ben-Dov *et al.*, The parathyroid is a target organ for FGF23 in rats. *The Journal of clinical investigation* **117**, 4003-4008 (2007).
29. T. Shimada *et al.*, Targeted ablation of Fgf23 demonstrates an essential physiological role of FGF23 in phosphate and vitamin D metabolism. *Journal of Clinical Investigation* **113**, 561-568 (2004).
30. A. Benet-Pagès, P. Orlik, T. M. Strom, B. Lorenz-Depiereux, An FGF23 missense mutation causes familial tumoral calcinosis with hyperphosphatemia. *Human Molecular Genetics* **14**, 385-390 (2005).
31. T. Larsson *et al.*, Fibroblast Growth Factor-23 Mutants Causing Familial Tumoral Calcinosis Are Differentially Processed. *Endocrinology* **146**, 3883-3891 (2005).
32. D. Sitara *et al.*, Genetic Ablation of Vitamin D Activation Pathway Reverses Biochemical and Skeletal Anomalies in Fgf-23-Null Animals. *The American Journal of Pathology* **169**, 2161-2170 (2006).
33. D. Sitara *et al.*, Homozygous ablation of fibroblast growth factor-23 results in hyperphosphatemia and impaired skeletogenesis, and reverses hypophosphatemia in Phex-deficient mice. *Matrix Biology* **23**, 421-432 (2004).
34. K. Kato *et al.*, Polypeptide GalNAc-transferase T3 and Familial Tumoral Calcinosis: SECRETION OF FIBROBLAST GROWTH FACTOR 23 REQUIRES O-GLYCOSYLATION. *Journal of Biological Chemistry* **281**, 18370-18377 (2006).
35. L. D. Quarles, Skeletal secretion of FGF-23 regulates phosphate and vitamin D metabolism. *Nat Rev Endocrinol* **8**, 276-286 (2012).
36. H. Komaba, M. Fukagawa, FGF23-parathyroid interaction: implications in chronic kidney disease. *Kidney Int* **77**, 292-298 (2009).
37. L. Craver *et al.*, Mineral metabolism parameters throughout chronic kidney disease stages 1–5—achievement of K/DOQI target ranges. *Nephrology Dialysis Transplantation* **22**, 1171-1176 (2007).
38. O. M. Gutiérrez *et al.*, Fibroblast Growth Factor 23 and Mortality among Patients Undergoing Hemodialysis. *New England Journal of Medicine* **359**, 584-592 (2008).
39. D. Fliser *et al.*, Fibroblast Growth Factor 23 (FGF23) Predicts Progression of Chronic Kidney Disease: The Mild to Moderate Kidney Disease (MMKD) Study. *Journal of the American Society of Nephrology* **18**, 2600-2608 (2007).

40. M. A. I. Mirza *et al.*, Circulating Fibroblast Growth Factor-23 Is Associated With Fat Mass and Dyslipidemia in Two Independent Cohorts of Elderly Individuals. *Arteriosclerosis, Thrombosis, and Vascular Biology* **31**, 219-227 (2011).
41. E. A. Imel, L. A. DiMeglio, S. L. Hui, T. O. Carpenter, M. J. Econs, Treatment of X-Linked Hypophosphatemia with Calcitriol and Phosphate Increases Circulating Fibroblast Growth Factor 23 Concentrations. *The Journal of Clinical Endocrinology & Metabolism* **95**, 1846-1850 (2010).
42. T. Georgoulas, S. Tournis, G. Lyritis, Changes of fibroblast growth factor 23 (FGF23) levels following calcitriol treatment in a vitamin D deficient patient. *Journal of musculoskeletal & neuronal interactions* **14**, 398-400 (2014).
43. S.-A. M. Burnett-Bowie *et al.*, Randomized Trial Assessing the Effects of Ergocalciferol Administration on Circulating FGF23. *Clinical Journal of the American Society of Nephrology* **7**, 624-631 (2012).
44. K. Wesseling-Perry, I. Salusky, Phosphate binders, vitamin D and calcimimetics in the management of chronic kidney disease–mineral bone disorders (CKD-MBD) in children. *Pediatr Nephrol* **28**, 617-625 (2013).
45. T. O. Carpenter *et al.*, Randomized trial of the anti-FGF23 antibody KRN23 in X-linked hypophosphatemia. *J Clin Invest* **124**, 1587-1597 (2014).
46. J. R. Stubbs, A. Idiculla, J. Slusser, R. Menard, L. D. Quarles, Cholecalciferol Supplementation Alters Calcitriol-Responsive Monocyte Proteins and Decreases Inflammatory Cytokines in ESRD. *Journal of the American Society of Nephrology* **21**, 353-361 (2010).
47. J. B. Wetmore, L. D. Quarles, Calcimimetics or vitamin D analogs for suppressing parathyroid hormone in end-stage renal disease: time for a paradigm shift? *Nat Clin Pract Neph* **5**, 24-33 (2009).
48. J. B. Wetmore, S. Liu, R. Krebill, R. Menard, L. D. Quarles, Effects of Cinacalcet and Concurrent Low-Dose Vitamin D on FGF23 Levels in ESRD. *Clinical Journal of the American Society of Nephrology* **5**, 110-116 (2010).
49. S. Wöhrle *et al.*, Pharmacological inhibition of fibroblast growth factor (FGF) receptor signaling ameliorates FGF23-mediated hypophosphatemic rickets. *Journal of Bone and Mineral Research* **28**, 899-911 (2013).
50. S. Wöhrle *et al.*, FGF receptors control vitamin D and phosphate homeostasis by mediating renal FGF-23 signaling and regulating FGF-23 expression in bone. *Journal of Bone and Mineral Research* **26**, 2486-2497 (2011).
51. C. Herbert *et al.*, Molecular mechanism of SSR128129E, an extracellularly acting, small-molecule, allosteric inhibitor of FGF receptor signaling. *Cancer Cell* **23**, 489-501 (2013).
52. R. Goetz *et al.*, Isolated C-terminal tail of FGF23 alleviates hypophosphatemia by inhibiting FGF23-FGFR-Klotho complex formation. *Proceedings of the National Academy of Sciences* **107**, 407-412 (2010).
53. R. Goetz *et al.*, Molecular Insights into the Klotho-Dependent, Endocrine Mode of Action of Fibroblast Growth Factor 19 Subfamily Members. *Molecular and Cellular Biology* **27**, 3417-3428 (2007).
54. V. S. Tagliabracci *et al.*, Dynamic regulation of FGF23 by Fam20C phosphorylation, GalNAc-T3 glycosylation, and furin proteolysis. *Proceedings of the National Academy of Sciences* **111**, 5520-5525 (2014).
55. J. J. Ward, L. J. McGuffin, K. Bryson, B. F. Buxton, D. T. Jones, The DISOPRED server for the prediction of protein disorder. *Bioinformatics* **20**, 2138-2139 (2004).
56. D. T. Jones, D. Cozzetto, DISOPRED3: precise disordered region predictions with annotated protein-binding activity. *Bioinformatics* **31**, 857-863 (2015).

57. X. Chen, C. H. Reynolds, Performance of similarity measures in 2D fragment-based similarity searching: comparison of structural descriptors and similarity coefficients. *J Chem Inf Comput Sci* **42**, 1407-1414 (2002).
58. D. Bajusz, A. Racz, K. Heberger, Why is Tanimoto index an appropriate choice for fingerprint-based similarity calculations? *J Cheminform* **7**, 20 (2015).
59. H. Kurosu *et al.*, Regulation of Fibroblast Growth Factor-23 Signaling by Klotho. *Journal of Biological Chemistry* **281**, 6120-6123 (2006).
60. M. Yamazaki *et al.*, Both FGF23 and extracellular phosphate activate Raf/MEK/ERK pathway via FGF receptors in HEK293 cells. *Journal of Cellular Biochemistry* **111**, 1210-1221 (2010).
61. D. F. Veber *et al.*, Molecular properties that influence the oral bioavailability of drug candidates. *J Med Chem* **45**, 2615-2623 (2002).
62. W. P. Walters, M. A. Murcko, Prediction of 'drug-likeness'. *Adv Drug Deliv Rev* **54**, 255-271 (2002).
63. C. A. Lipinski, Lead- and drug-like compounds: the rule-of-five revolution. *Drug Discov Today Technol* **1**, 337-341 (2004).
64. C. A. Lipinski, F. Lombardo, B. W. Dominy, P. J. Feeney, Experimental and computational approaches to estimate solubility and permeability in drug discovery and development settings. *Adv Drug Deliv Rev* **46**, 3-26 (2001).
65. A. K. Ghose, V. N. Viswanadhan, J. J. Wendoloski, A knowledge-based approach in designing combinatorial or medicinal chemistry libraries for drug discovery. 1. A qualitative and quantitative characterization of known drug databases. *J Comb Chem* **1**, 55-68 (1999).
66. I. Muegge, Pharmacophore features of potential drugs. *Chemistry* **8**, 1976-1981 (2002).
67. H. A. Carlson, J. A. McCammon, Accommodating protein flexibility in computational drug design. *Mol Pharmacol* **57**, 213-218 (2000).
68. H. A. Carlson, J. A. McCammon, Accommodating Protein Flexibility in Computational Drug Design. *Molecular Pharmacology* **57**, 213-218 (2000).
69. J.-H. Lin, A. L. Perryman, J. R. Schames, J. A. McCammon, Computational Drug Design Accommodating Receptor Flexibility: The Relaxed Complex Scheme. *Journal of the American Chemical Society* **124**, 5632-5633 (2002).
70. J. A. McCammon, Target flexibility in molecular recognition. *Biochimica et Biophysica Acta (BBA) - Proteins and Proteomics* **1754**, 221-224 (2005).
71. J. Q. Feng *et al.*, Loss of DMP1 causes rickets and osteomalacia and identifies a role for osteocytes in mineral metabolism. *Nature genetics* **38**, 1310-1315 (2006).
72. S. Liu *et al.*, Pathogenic role of Fgf23 in Dmp1-null mice. *Am J Physiol Endocrinol Metab* **295**, E254-261 (2008).
73. B. L. Batley *et al.*, Inhibition of FGF-1 receptor tyrosine kinase activity by PD 161570, a new protein-tyrosine kinase inhibitor. *Life Sci* **62**, 143-150 (1998).
74. A. M. Thompson *et al.*, 3-(3,5-Dimethoxyphenyl)-1,6-naphthyridine-2,7-diamines and related 2-urea derivatives are potent and selective inhibitors of the FGF receptor-1 tyrosine kinase. *J Med Chem* **43**, 4200-4211 (2000).
75. J. Ho *et al.*, Molecular recognition of ketamine by a subset of olfactory G protein–coupled receptors. *Science signaling* **8**, ra33-ra33 (2015).
76. K. Kapoor *et al.*, Discovery of Novel Non-active Site Inhibitors of the Prothrombinase Enzyme Complex. *Journal of Chemical Information and Modeling*, (2016).
77. S. Wohrle *et al.*, FGF receptors control vitamin D and phosphate homeostasis by mediating renal FGF-23 signaling and regulating FGF-23 expression in bone. *J Bone Miner Res* **26**, 2486-2497 (2011).

78. S. Wohrle *et al.*, Pharmacological inhibition of fibroblast growth factor (FGF) receptor signaling ameliorates FGF23-mediated hypophosphatemic rickets. *J Bone Miner Res* **28**, 899-911 (2013).
79. T. O. Carpenter *et al.*, Randomized trial of the anti-FGF23 antibody KRN23 in X-linked hypophosphatemia. *The Journal of Clinical Investigation* **124**, 1587-1597 (2014).
80. Y. Aono *et al.*, Therapeutic effects of anti-FGF23 antibodies in hypophosphatemic rickets/osteomalacia. *J Bone Miner Res* **24**, 1879-1888 (2009).
81. M. Mohammadi, R. GOETZ. (Google Patents, 2013).
82. A. Biegert, C. Mayer, M. Remmert, J. Söding, A. N. Lupas, The MPI Bioinformatics Toolkit for protein sequence analysis. *Nucleic Acids Research* **34**, W335-W339 (2006).
83. J. Söding, A. Biegert, A. N. Lupas, The HHpred interactive server for protein homology detection and structure prediction. *Nucleic Acids Research* **33**, W244-W248 (2005).
84. N. J. Harmer, L. Pellegrini, D. Chirgadze, J. Fernandez-Recio, T. L. Blundell, The Crystal Structure of Fibroblast Growth Factor (FGF) 19 Reveals Novel Features of the FGF Family and Offers a Structural Basis for Its Unusual Receptor Affinity†,‡. *Biochemistry* **43**, 629-640 (2004).
85. S. K. Olsen *et al.*, Fibroblast Growth Factor (FGF) Homologous Factors Share Structural but Not Functional Homology with FGFs. *Journal of Biological Chemistry* **278**, 34226-34236 (2003).
86. N. Eswar *et al.*, in *Current Protocols in Bioinformatics*. (John Wiley & Sons, Inc., 2002).
87. S. Jo, T. Kim, V. G. Iyer, W. Im, CHARMM-GUI: A web-based graphical user interface for CHARMM. *Journal of Computational Chemistry* **29**, 1859-1865 (2008).
88. B. R. Brooks *et al.*, CHARMM: The biomolecular simulation program. *Journal of Computational Chemistry* **30**, 1545-1614 (2009).
89. A. T. Brünger, M. Karplus, Polar hydrogen positions in proteins: Empirical energy placement and neutron diffraction comparison. *Proteins: Structure, Function, and Bioinformatics* **4**, 148-156 (1988).
90. G. Arfken, Mathematical Methods for Physicists. 428-436 (1985).
91. J.-W. Chu, B. L. Trout, B. R. Brooks, A super-linear minimization scheme for the nudged elastic band method. *The Journal of Chemical Physics* **119**, 12708-12717 (2003).
92. J.-P. Ryckaert, G. Ciccotti, H. J. C. Berendsen, Numerical integration of the cartesian equations of motion of a system with constraints: molecular dynamics of n-alkanes. *Journal of Computational Physics* **23**, 327-341 (1977).
93. A. Raval, S. Piana, M. P. Eastwood, R. O. Dror, D. E. Shaw, Refinement of protein structure homology models via long, all-atom molecular dynamics simulations. *Proteins: Structure, Function, and Bioinformatics* **80**, 2071-2079 (2012).
94. R. Brenke *et al.*, Fragment-based identification of druggable 'hot spots' of proteins using Fourier domain correlation techniques. *Bioinformatics* **25**, 621-627 (2009).
95. B. J. Grant *et al.*, Novel Allosteric Sites on Ras for Lead Generation. *PLoS ONE* **6**, e25711 (2011).
96. Y. Miao, S. E. Nichols, J. A. McCammon, Mapping of Allosteric Druggable Sites in Activation-Associated Conformers of the M2 Muscarinic Receptor. *Chemical Biology & Drug Design* **83**, 237-246 (2014).
97. D. Riccardi, J. M. Parks, A. Johs, J. C. Smith, HackaMol: An Object-Oriented Modern Perl Library for Molecular Hacking on Multiple Scales. *Journal of Chemical Information and Modeling* **55**, 721-726 (2015).
98. J. J. Irwin, B. K. Shoichet, ZINC − A Free Database of Commercially Available Compounds for Virtual Screening. *Journal of Chemical Information and Modeling* **45**, 177-182 (2005).
99. T. Tanimoto. (McGraw-Hill New York, 1968).
100. N. M. OLBoyle *et al.*, Open Babel: An open chemical toolbox. *J Cheminf* **3**, 33 (2011).
101. N. M. O'Boyle, Towards a Universal SMILES representation-A standard method to generate canonical SMILES based on the InChI. *J. Cheminformatics* **4**, 22 (2012).

102. M. F. Sanner, Python: a programming language for software integration and development. *J Mol Graph Model* **17**, 57-61 (1999).
103. O. Trott, A. J. Olson, AutoDock Vina: Improving the speed and accuracy of docking with a new scoring function, efficient optimization, and multithreading. *Journal of Computational Chemistry* **31**, 455-461 (2010).
104. E. J. Weinman, D. Steplock, S. Shenolikar, R. Biswas, Fibroblast growth factor-23-mediated inhibition of renal phosphate transport in mice requires sodium-hydrogen exchanger regulatory factor-1 (NHERF-1) and synergizes with parathyroid hormone. *J Biol Chem* **286**, 37216-37221 (2011).
105. Z. Xiao *et al.*, Osteocyte-specific deletion of Fgfr1 suppresses FGF23. *PLoS One* **9**, e104154 (2014).
106. R. Salomon-Ferrer, D. A. Case, R. C. Walker, An overview of the Amber biomolecular simulation package. *Wiley Interdisciplinary Reviews: Computational Molecular Science* **3**, 198-210 (2013).
107. V. Hornak *et al.*, Comparison of multiple Amber force fields and development of improved protein backbone parameters. *Proteins: Structure, Function, and Bioinformatics* **65**, 712-725 (2006).
108. W. D. Cornell *et al.*, A Second Generation Force Field for the Simulation of Proteins, Nucleic Acids, and Organic Molecules. *Journal of the American Chemical Society* **117**, 5179-5197 (1995).
109. M. R. Hestenes, E. Stiefel, Methods of conjugate gradients for solving linear systems. (1952).
110. D. Case *et al.*, AMBER 12. *University of California, San Francisco* **1**, (2012).
111. D. Kozakov *et al.*, The FTMap family of web servers for determining and characterizing ligand-binding hot spots of proteins. *Nat Protoc* **10**, 733-755 (2015).
112. C. H. Ngan *et al.*, FTMAP: extended protein mapping with user-selected probe molecules. *Nucleic Acids Res* **40**, W271-275 (2012).
113. D. R. Hall, C. H. Ngan, B. S. Zerbe, D. Kozakov, S. Vajda, Hot Spot Analysis for Driving the Development of Hits into Leads in Fragment-Based Drug Discovery. *Journal of Chemical Information and Modeling* **52**, 199-209 (2012).